JOURNAL OF PROPULSION AND POWER
Vol. 11, No. 1, January–February 1995

Low-Density Nozzle Flow by the Direct Simulation Monte Carlo and Continuum Methods

Chan-Hong Chung,* Suk C. Kim,† and Robert M. Stubbs‡
NASA Lewis Research Center, Cleveland, Ohio 44135
and
Kenneth J. De Witt§
University of Toledo, Toledo, Ohio 43606

Two different approaches, the direct simulation Monte Carlo (DSMC) method based on molecular gasdynamics, and a finite-volume approximation of the Navier-Stokes equations, which are based on continuum gasdynamics, are employed in the analysis of a low-density gas flow in a small converging-diverging nozzle. The fluid experiences various kinds of flow regimes including continuum, slip, transition, and free-molecular. Results from the two numerical methods are compared with Rothe's experimental data, in which density and rotational temperature variations along the centerline and at various locations inside a low-density nozzle were measured by the electron-beam fluorescence technique. The continuum approach showed good agreement with the experimental data as far as density is concerned. The results from the DSMC method showed good agreement with the experimental data, both in the density and the rotational temperature. It is also shown that the simulation parameters, such as the gas/surface interaction model, the energy exchange model between rotational and translational modes, and the viscosity-temperature exponent, have substantial effects on the results of the DSMC method.

Introduction

THE mission performance of satellites and spacecraft such as on-orbit lifetimes, payloads, and trip times are significantly impacted by low-thrust rocket engines that are used for the control of altitude and trajectory of the vehicles. Another important factor affecting the mission performance is the contamination of sensitive instruments and system components of the vehicles in the plume and backflow region of the thrusters. Hence, the understanding of the detailed flow structure inside low-thrust rocket nozzles is very important for the accurate prediction of the thrust and mass flow levels, and also for the precise analysis of the plume and backflow.

For this type of rocket engine, due to the small thrust level, nozzle scales are quite small and reservoir pressures are very low. Reynolds numbers of the flow in the nozzle are very low and rarefaction effects can significantly alter the internal flow structure in the vacuum of the space environment. Under these conditions, the flow exhibits strong nonequilibrium effects, such as slip at the wall, due to rapid expansion into the low-density environment. The fluid experiences continuum, transition, and free-molecular flow regimes. Consequently, conventional continuum gasdynamics that are based on the concept of a local equilibrium may not be adequate, and an approach based on molecular gasdynamics is required for the analysis of the flow.

Even though there exist many methods in molecular gasdynamics to analyze low-density gas flows, the majority of the works investigating this type of expanding flow employ the direct simulation Monte Carlo (DSMC) method of Bird.[1] Several DSMC investigations that have dealt with this aspect include those by Bird,[2,3] Heuser et al.,[4] Campbell,[5,6] Nelson and Doo,[7] Penko et al.,[8] Boyd et al.,[9] and Zelesnik et al.[10] The DSMC method is a computer simulation technique to solve Boltzmann's equation by modeling a real gas flow using a representative set of molecules. However, due to intensive computational requirements, current applications of the DSMC method are generally limited to near continuum and rarefied flows. Continuum methods are usually much more efficient than the DSMC method for high and normal density flows. Thus, in the analysis of flows that involve both continuum and rarefied flow regimes, it would be reasonable to combine both methods. The simplest utilization of both methods is to solve rarefied flow regimes using the DSMC method by obtaining boundary conditions from the solution of continuum methods. This, indeed, is the most widely used method in analyzing the flows that involve both continuum and rarefied flow regimes.

In the present study, two different approaches, the DSMC method based on molecular gasdynamics, and a finite volume approximation of the Navier-Stokes equations, which are based on continuum gasdynamics, are employed in the analysis of the internal flow structure in a small converging-diverging nozzle. The full Navier-Stokes equations are solved by a lower-upper symmetric successive over-relaxation (LU-SSOR) scheme developed by Yoon and Shuen[11] in the RPLUS code.[12] In the DSMC simulation, the boundary conditions for the solution domain are obtained from the results of the Navier-Stokes solution. Detailed numerical results from the two approaches, such as density and temperature inside the nozzle, are compared with Rothe's[13] experimental data.

Few experimental data are available for this type of low-thrust nozzle, and most data deal with gross characteristics of nozzle performance such as thrust levels and discharge coefficients. This type of data does not provide detailed information regarding the internal flow structure. Rothe's work is probably the only one in which detailed low-density flow properties have been measured inside a nozzle using the electron-

Presented as Paper 93-0727 at the AIAA 31st Aerospace Sciences Meeting and Exhibit, Reno, NV, Jan. 11–14, 1993; received Feb. 10, 1993; revision received May 25, 1994; accepted for publication July 1, 1994.

*Resident Research Associate, Computational Methods for Space Branch. Member AIAA.
†Senior Research Engineer, NYMA, Inc., Lewis Research Center Group. Member AIAA.
‡Chief, Computational Methods for Space Branch. Senior Member AIAA.
§Professor, Department of Chemical Engineering. Member AIAA.

beam fluorescence technique. In addition to Rothe's work, low-density pitot pressure measurements together with numerical simulations were performed by Penko et al.[8] and Boyd et al.[9] They compared continuum and DSMC results with pitot pressure data at the nozzle exit plane and at various locations in the plume region. Comparison between the DSMC and continuum results was also made by Penko and Boyd for the flow inside the nozzle. Campbell,[5,6] Nelson and Doo,[7] and Zelesnik et al.[10] have also considered expanding low-density flows using the DSMC method, and compared their results with experimental data, but in these investigations no comparison was made with experimental data inside the nozzles.

The present study reports, for the first time, a detailed assessment of the DSMC method for low-density internal flows by comparison with experimental data. The validity of the numerical methods, the DSMC and continuum methods, has been assessed by comparing simulation results with detailed measurements such as density and rotational temperature at various locations inside the low-thrust nozzle. In addition, special attention is paid to the DSMC simulation parameters, such as the gas/surface interaction model and the energy exchange model between rotational and translational modes.

Problem Statement

For the analysis of low-density nozzle flow, Rothe's[13] experiment is chosen as a reference problem due to the availability of detailed measurements inside the nozzle. Figure 1 illustrates the geometry of the nozzle used in Rothe's experiment and in the present numerical analysis. The nozzle is made of graphite to reduce optical reflections and to minimize backscattering and secondary emission of electrons. The subsonic and supersonic portions of the nozzle are cones having half-angles of 30 and 20 deg, respectively, with longitudinal radii of curvature at the throat equal to one-half of the throat radius. The maximum area ratio at the exit based on the throat area is 66. The computational domain for the continuum method consists of the nozzle interior (OAFI), and the region extends upstream an axial distance of 10 mm from the nozzle throat (OK). The shaded region in the lower portion of Fig. 1 indicates the DSMC simulation domain. The length of the curved nozzle contour (IH) is about 0.5 mm. The simulation domain extends to an axial distance of 14 mm from the nozzle exit plane (AB), to a radial distance of 14 mm from the nozzle lip (FD), and to an axial distance of 14 mm from the nozzle exit plane into the backflow region (DE). The inflow boundary is located at the nozzle throat (OI). Supersonic outflow boundary conditions are assumed along the outflow boundary (BC, CE, and EG). The test gas is nitrogen with a stagnation temperature of $T_0 = 300$ K. The flow conditions are listed in Table 1. In the table, the throat Reynolds number, $Re_t = 2\dot{m}/\pi\mu_0 R_t$, is based on the viscosity at the stagnation chamber condition μ_0. Here, the quantity $\dot{m}$ is the mass flow rate, and R_t is the throat radius. The Knudsen number is based on the throat diameter and the stagnation chamber condition.

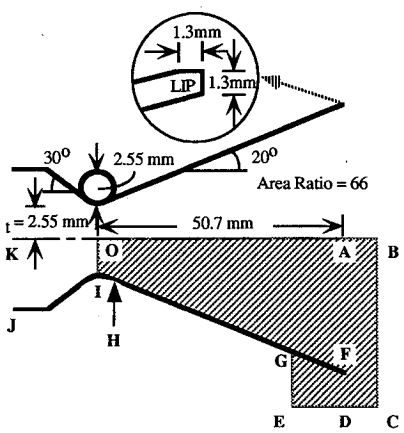

Fig. 1 Geometry of low-thrust nozzle.

Continuum Method

In the continuum method, the Navier-Stokes equations are solved by the LU-SSOR scheme[11] in the RPLUS code.[12] The code employs an implicit finite volume LU-SSOR scheme to solve the full Navier-Stokes equations and the species equations in a fully coupled manner. The LU-SSOR scheme employs an implicit Newton iteration technique to solve the finite volume approximation of the steady-state version of the governing equations. Even though the system of equations is formulated in a fully implicit and a fully coupled manner, the LU-SSOR scheme requires only scalar diagonal inversion for the flow equations. This results in a fast convergence rate, and the convergence of the Newton iteration method is assured by the diagonal dominance of the coefficient matrices of the LU-SSOR scheme. The code has been applied to various rocket nozzles including H_2/O_2 thrusters,[14,15] nuclear thermal rockets,[16] and low-thrust nozzles.[17]

In the present study, the inflow total enthalpy and pressure are assumed to be constant. At the inlet of the nozzle (KJ in Fig. 1), the radial velocity is assumed to be zero and the axial velocity is obtained by extrapolation from the interior. The temperature is obtained from the inflow total enthalpy and the velocity. The pressure and density are obtained from the isentropic relation and the equation of state, respectively. At the exit of the nozzle where the flow is mostly supersonic, all dependent variables are extrapolated from the interior. The wall is assumed to be adiabatic and the no-slip condition is used at the wall. At the axis of symmetry, the radial velocity and the radial derivatives of the other dependent variables are set to zero. The calculations are made with a 240 × 60 grid. A very small uniform axial grid is used from the inlet to some distance downstream of the throat, after which the grid spacing increases. The radial grid size becomes finer near the wall. A detailed description of the continuum method used in the present study can be found in Ref. 17.

Figure 2 shows profiles of flow variables at the nozzle throat obtained from the continuum solution that are used for the input boundary condition in the DSMC simulations. Here the quantities ρ, U_r, U_x, T, and S are density, radial velocity, axial velocity, temperature, and the most probable thermal speed, $S = \sqrt{2RT}$, respectively. The subscript, 0, denotes the stagnation chamber condition.

Table 1 Flow conditions

Test gas	N_2
Stagnation temperature, T_0	300 K
Stagnation pressure, P_0	474 Pa
Wall temperature, T_W	300 K
Reynolds number, Re_t	270
Knudsen number, Kn	2.3×10^{-3}

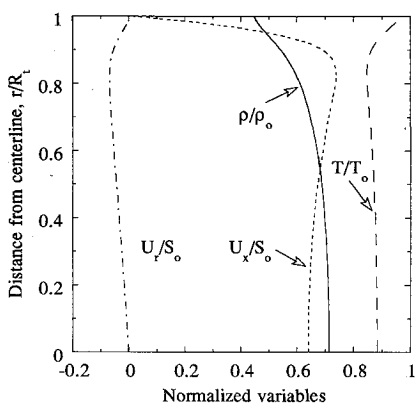

Fig. 2 Profiles of flow variables at the nozzle throat used for input to the DSMC simulations.

DSMC Method

The DSMC method is a popular simulation technique for low-density flows, and the DSMC code used in the present study is based on the same principles as described in Bird,[1] together with the variable hard sphere (VHS) model[18] as a molecular model, and the no time counter (NTC) method[19] as a collision-sampling technique. The code has been developed at the NASA Lewis Research Center to investigate various low-density flows of gas mixtures in arbitrary shaped flow domains, with or without chemical reactions.[20-22] Details of the code and computation may be found in Ref. 20.

The VHS exponent ω of nitrogen is chosen to be 0.24, with the reference molecular diameter of 4.07×10^{-10} m at the reference temperature 273 K.[19] Chemical reactions and the vibrational mode are assumed to be frozen. For the calculation of rotational energy exchange between the colliding molecules, the Borgnakke-Larsen phenomenological model[23] is employed together with the temperature-dependent energy exchange probability of Boyd.[24] However, the temperature-dependent energy exchange probability is modified to be consistent with the experimental data for the rotational relaxation of nitrogen obtained by various methods and compatible with the VHS model. The modification employed in the present study is described below.

In the Larsen-Borgnakke phenomenological model, a fraction ϕ of translational collisions are assumed to be inelastic, and the rest of the collisions are considered as elastic. Hence, the fraction ϕ can be interpreted as the average probability of rotational energy exchange for translational collisions. The rotational collision number Z_R is usually defined by

$$Z_R = (\tau_R/\tau_t) \tag{1}$$

where the quantity τ_R is the rotational relaxation time, and τ_t is the mean collision time for translational relaxation. The rotational collision number is the average number of molecular collisions that are required for rotational-translational energy exchange. Therefore, the average probability of rotational energy exchange for translational collisions ϕ, can be given as the inverse of the rotational collision number:

$$\phi = (1/Z_R) \tag{2}$$

As is the case in Boyd,[24] the rotational collision number may be obtained from Parker's expression[25] by determining the constants to match available experimental data and the more rigorous analysis of Lordi and Mates.[26] It should be noted here that special attention should be paid in the interpretation of experimental data due to the use of different mean collision times for translational relaxation in presenting the experimental data. Also, these data must be corrected so that they should be compatible with the VHS model

$$Z_{R,\mathrm{VHS}} = F_c Z_R \tag{3}$$

where the quantity $Z_{R,\mathrm{VHS}}$ is the rotational collision number suitable for the VHS model, and F_c is a correction factor that is given by

$$F_c = (\tau_t/\tau_{t,\mathrm{VHS}}) \tag{4}$$

where the quantity $\tau_{t,\mathrm{VHS}}$ is the mean collision time for translational relaxation for the VHS model. If τ_t is given by $\pi\mu/(4P)$, which is one of the most widely used mean collision times,[27] it can be shown that the correction factor is given by

$$F_c = \frac{15\alpha\pi\Gamma(2-\omega)}{8\Gamma(4-\omega)} \tag{5}$$

where the quantity α is the correction factor to the first approximation of the coefficient of viscosity,[19] and Γ denotes the gamma function. The value of the correction factor is in a range of 0.996–1.571, depending on the molecular model.

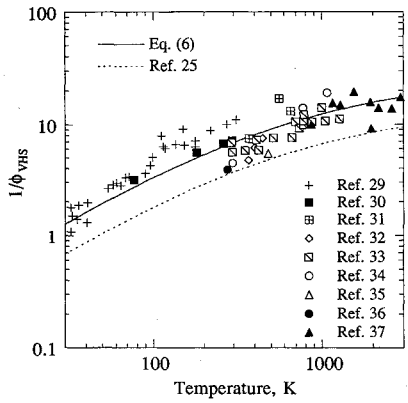

Fig. 3 Temperature-dependent rotational energy exchange probability for the VHS model.

Then, the temperature-dependent rotational energy exchange probability suitable for the VHS model is given by

$$\frac{1}{\phi_{\mathrm{VHS}}} = Z_{R,\mathrm{VHS}} = \frac{F_c(Z_R)^{\infty}}{1 + \dfrac{\pi^{3/2}}{2}(T^*/T)^{1/2} + [(\pi^2/4) + 2](T^*/T)} \tag{6}$$

where the quantity T^* is the characteristic temperature of the intermolecular potential, and $(Z_R)^{\infty}$ is the limiting value. A small numerical correction to Parker's expression noted by Brau and Jonkman[28] is included in Eq. (6). Figure 3 shows various experimental data[29-37] in a temperature range from 30–3000 K for N_2 corrected according to Eq. (3). The solid line represents Eq. (6) with the correction factor from Eq. (5) for $T^* = 91.5$ K, $Z_R^{\infty} = 23.5$, and $\omega = 0.24$. The temperature-dependent rotational energy exchange probability employed by Boyd[24] is also shown in the figure.

Employing the method introduced by Boyd,[24] Eq. (6) may be converted into the following instantaneous exchange probability suitable for the VHS model:

$$\phi_{\mathrm{VHS}}(Z_R)^{\infty}F_c = 1 + \frac{\Gamma(\zeta + 2 - \omega)}{\Gamma(\zeta + 3/2 - \omega)}\left(\frac{kT^*}{E_c}\right)^{1/2}\frac{\pi^{3/2}}{2} + \frac{\Gamma(\zeta + 2 - \omega)}{\Gamma(\zeta + 1 - \omega)}\left(\frac{kT^*}{E_c}\right)\left(\frac{\pi^2}{4} + 2\right) \tag{7}$$

where the quantity ζ is the average internal DOF of the colliding molecules, k is the Boltzmann constant, and E_c is the collision energy.

A diffusely reflecting wall with 10% thermal accommodation is assumed for the interaction between the gas molecules and the wall. For comparison, several gas/surface interaction models are also considered, including diffuse reflection with full thermal accommodation, specular reflection, adiabatic wall, and a combination of the three models. The energy exchange between rotational and translational modes when the molecules collide with the surface involves quite complex physical processes. Also, these energy exchange mechanisms largely depend on the kind of gas molecules and the wall materials. One of the interesting examples is the interaction between a graphite surface and NO or Br_2.[38] In this case, the rotational temperature of the reflecting gases never exceeds 250 K, independent of the surface temperature above 300 K due to the strong rotational cooling effect. Due to the lack of experimental data between graphite and nitrogen, the wall is assumed to be a monatomic gas with an infinite mass for the rotational-translational energy exchange of the reflecting molecules, and the probability is assumed to be given by Eq.

(7). For comparison, full thermal accommodation of rotational energy at the wall is also considered.

Results and Discussion

To present the general idea regarding the differences between the continuum and DSMC methods and the overall structure of the flowfield, density and Mach number contours obtained by the two methods will be considered first. Figure 4 shows density contours obtained by the two methods. The DSMC solution occupies the upper portion of the figure, and the continuum solution is shown in the lower portion. The density is normalized by the stagnation chamber density ρ_0, and plotted in a logarithmic scale with base 10. It can be seen that the density profiles near the throat exhibit a density ridge where the density is higher than on the axis. The density humps indicate a weak compression wave originating near the throat where the wall curvature changes abruptly. The DSMC method predicts a weaker compression than the continuum method. In the entire flowfield, the density obtained by the DSMC method is lower than that obtained by the continuum method. The fluid experiences about two orders of magnitude decrease in density across the nozzle, and about 5 orders of magnitude in the backflow region at the plane parallel to the exit. In some parts of the backflow region, a severe scattering of data in the results of the DSMC method appeared if the normalized density is lower than 10^{-6}, which made it difficult to interpret the results there. Hence, the density contours are plotted up to 10^{-6}. Some wiggles in the contours are due to the scattering of the data, the interpolating schemes used in the plotting software, and the larger cell size in this region.

Figure 5 shows the Mach contours obtained by the two methods. Again, the DSMC solution occupies the upper portion of the figure, and the continuum solution is shown in the lower portion. Along the axis, the DSMC method predicts higher Mach numbers than the continuum method. This means the DSMC method predicts a slightly faster expansion of the flow, i.e., lower density and temperature, than does the continuum method. It also can be seen that the DSMC method predicts the turning of the flow toward the nozzle lip and the termination of the sonic line of the internal boundary layer. This is consistent with previous observations—experimentally,[39] analytically,[40] and from DSMC simulation results[2]—that if the flow is highly underexpanded the effect of the very high-pressure gradient at the nozzle lip is to accelerate the subsonic portion of the boundary layer. This results in the intersection of the sonic line with the nozzle lip. Another difference between the two methods is that the DSMC method predicts a much thinner subsonic layer near the nozzle wall due to velocity slip. The accurate analysis of the flow structure in the boundary layer near the nozzle lip is very important in the prediction of plume backflow. This is because the flow in the nozzle wall boundary layer near the nozzle lip is the origin of the plume backflow, and is, thus, the most important factor affecting the flow structure in the plume backflow.

Consideration is now given to the detailed flow structure inside the nozzle. In Fig. 6 density profiles along the centerline of the nozzle obtained by the continuum and the DSMC methods together with the experimental data of Rothe are shown. Densities are normalized by the stagnation value ρ_0, and the axial distance, which is measured from the nozzle throat, is normalized by the throat radius. The results from both the continuum and the DSMC methods show good agreement with Rothe's experimental data. The maximum uncertainty limit of the experiment for the density data along the centerline reported by Rothe[41] is $\pm 10\%$. Figure 7 shows temperature profiles along the centerline of the nozzle obtained by the continuum and the DSMC methods together with the experimental data. Temperatures are normalized by the stagnation value T_0. In the continuum method that is based on the concept of local equilibrium, the flow is represented by only one equilibrium temperature, while the DSMC method gives both translational and rotational temperatures. Due to the fast expansion, the rotational temperature is always higher than the translational temperature along the axis, and it can

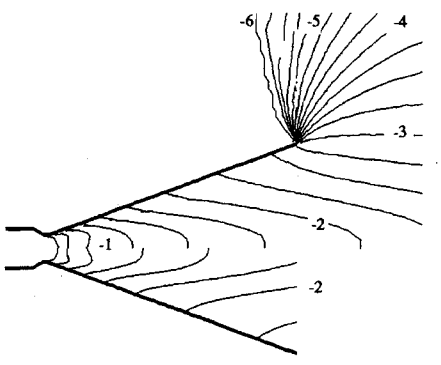

Fig. 4 Comparison of density contours, $\log_{10}(\rho/\rho_0)$, obtained by the continuum (lower) and DSMC (upper) method.

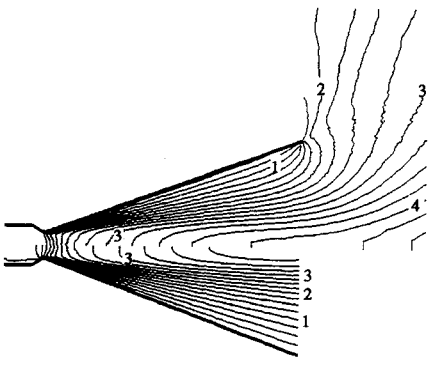

Fig. 5 Comparison of Mach number contours obtained by the continuum (lower) and DSMC (upper) method.

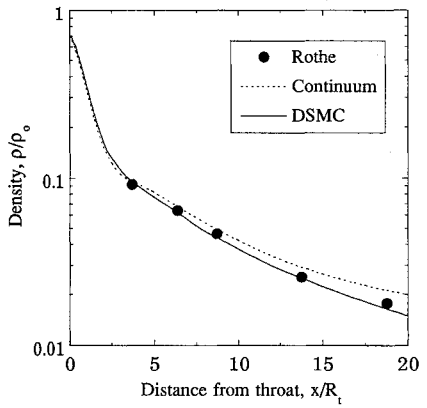

Fig. 6 Comparison of density variation along the nozzle centerline.

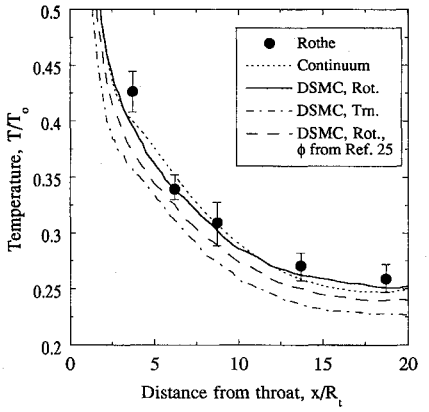

Fig. 7 Comparison of temperature variation along the nozzle centerline.

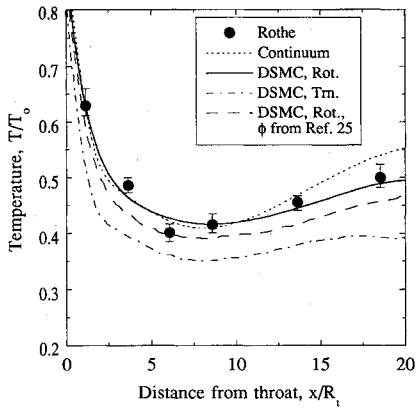

Fig. 8 Comparison of temperature variation along the nozzle centerline for P_0 = 209 Pa.

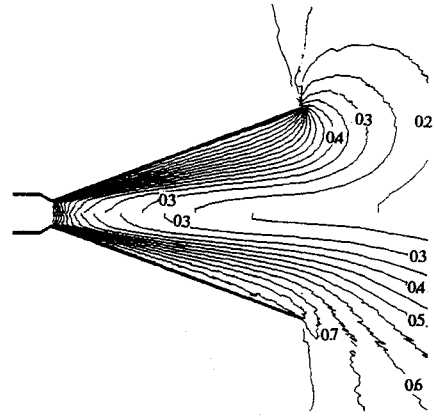

Fig. 9 Comparison of temperature contours T/T_0 obtained by the DSMC method. Rotational (lower) and translational (upper).

be seen that the rotational temperature obtained by the DSMC method matches Rothe's experimental data. It should be noted here that the temperature measured by Rothe is the rotational temperature. To compare the effect of the rotational energy exchange probability, the rotational temperature obtained by using the instantaneous energy exchange probability employed by Boyd[9,24] is also shown in the figure. It can be seen that the introduction of the correction factor, which is consistent with experimental data and compatible with the VHS model, results in a higher rotational temperature and gives better agreement with Rothe's experimental data. The effect of the correction factor is more accentuated as the flow becomes more rarefied. Figure 8 shows temperature profiles along the centerline of the nozzle obtained by the continuum and the DSMC methods together with the experimental data for the case of P_0 = 209 Pa, which is about 2.3 times lower stagnation chamber pressure than that of the reference problem. In this lower pressure case, a quite different flow structure from the higher pressure case can be observed. In the higher pressure case, the axial temperatures decrease monotonically from the throat to the nozzle exit, whereas in the lower pressure case the temperatures pass through a minimum and then increase toward the nozzle exit due to rarefaction effects. That is, as the flow becomes more rarefied, the effect of molecule-surface collisions increases while that of molecule-molecule collisions decreases. From a continuum point of view, this means there is an increase of the thermalization of the flow energy by viscous dissipation. The rotational temperature obtained from the present DSMC calculation shows good agreement with the measured rotational temperature except for the minimum point. All the numerical methods predict the location of the minimum at $x/R_t \cong 8$, while that in the experiment occurs at $x/R_t \cong 6$. The experimental error bars in Figs. 7 and 8 are random errors only, which are based on the signal-to-noise ratio in the rotational spectra.[13] Significant differences can be clearly seen from the comparison with the measured rotational temperature. Although not shown, there is no appreciable difference in the translational temperature due to the change in the rotational energy exchange probability.

Figure 9, in which contours of the two temperatures obtained by the DSMC method are shown, demonstrates the degree of thermal nonequilibrium between the translational and rotational modes. The translational temperature occupies the upper portion of the figure, and the rotational temperature is shown in the lower portion. Temperatures are normalized by the stagnation value T_0. The translational temperature drops faster than the rotational temperature along the axis. A remarkable difference between the two temperatures occurs around the nozzle lip where the flow rapidly expands around the corner. In this region, the rotational temperature becomes almost frozen due to the rapid expansion into vacuum.

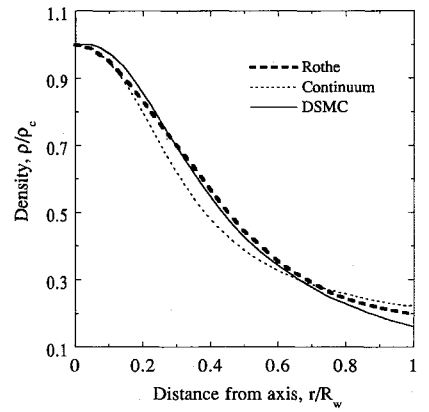

Fig. 10 Comparison of density profiles at the plane near the exit.

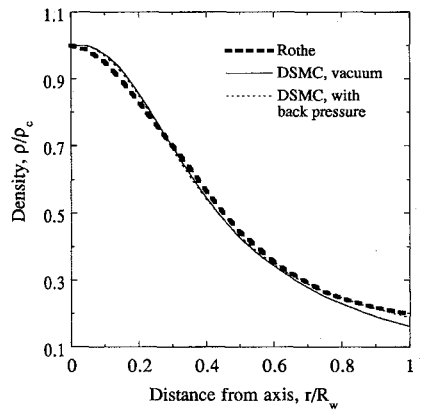

Fig. 11 Effect of background pressure on the density profile at the plane near the exit.

Comparison between the continuum and DSMC methods is now made in the plane near the nozzle exit. Figure 10 shows density profiles at x/R_t = 18.7, 3 mm inside from the exit, obtained by the continuum and the DSMC methods together with the experimental data of Rothe. Densities are normalized by the value at the axis ρ_c, and the r distance is normalized by the nozzle radius at the location R_w. It can be seen that as the flow comes close to the nozzle exit, the inviscid core almost vanishes and a boundary layer occupies the whole cross section of the nozzle. The results from both the continuum and the DSMC methods show relatively good agreement with Rothe's experimental data. The slight underprediction of the density near the nozzle wall in the DSMC result is due to the effect of ambient pressure. The effect of the background pressure is demonstrated in Fig. 11 where the DSMC result with a finite background pressure is shown. To investigate the

effect of the ambient pressure, the pressure along the outflow boundaries (CE and EG in Fig. 1) is assumed to be 1/310 P_0, which is the actual ambient pressure in Rothe's experiment. Although the boundaries used in the present calculation may not be far enough from the exit and the nozzle lip for an accurate result, it is believed that this will give a rough estimation of the effect of the ambient pressure. It can be seen that the effect of applying this ambient pressure increases the density near the nozzle lip and makes it coincide with the experimental data, while it has a negligible effect on the flow around the axis.

In Fig. 12 density profiles obtained by the two methods at various locations inside the nozzle together with the experimental data are compared. The density is normalized by the stagnation value. Rothe's experimental data is calculated from his centerline density and cross-sectional densities normalized

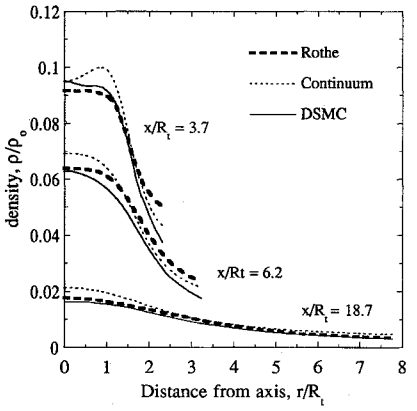

Fig. 12 Comparison of density profiles at various locations inside the nozzle.

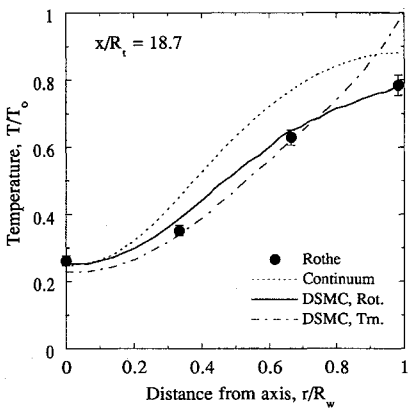

Fig. 13 Comparison of temperature profiles at the plane near the exit.

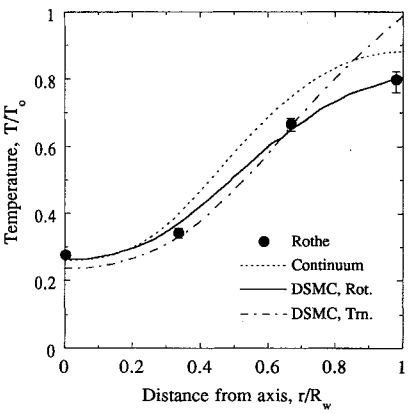

Fig. 14 Comparison of temperature profiles.

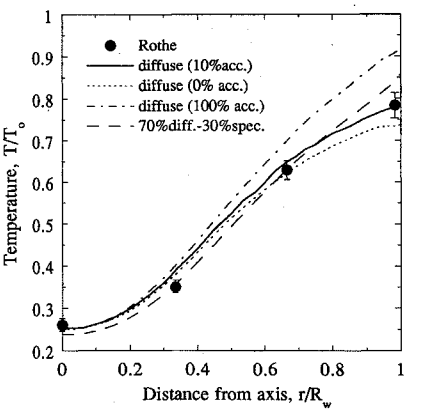

Fig. 15 Effect of wall interaction models on the rotational temperature profiles at the plane near the exit.

by the centerline density. As discussed earlier, the density profiles obtained by the two numerical methods show humps at $x/R_t = 3.7$, while the experimental data is flat. Except for the region near the wall and the large hump in the continuum result near the throat, the agreement between the calculations and the experimental data can be considered fair. The poor performance of the numerical results near the wall is a subject of future studies. However, it should be noted here that, in order to convert beam intensity to gas density, a knowledge of the electron beam current at the point of measurement is required.[41] This requirement poses a problem near the wall due to backscattering and secondary emission of electrons at the nozzle surface, and can lower the accuracy of the result near the wall. At higher pressure levels collisional quenching effects cannot be neglected, and this also can lower the accuracy of the experimental data near the throat.

Figures 13 and 14 show temperature profiles at $x/R_t = 18.7$, 3 mm inside from the nozzle exit, and at $x/R_t = 13.7$, respectively, obtained by the continuum and the DSMC methods together with the experimental data. Temperatures are normalized by the stagnation value T_0. The stagnation value is almost recovered in the translational temperature obtained by the DSMC method near the wall, while in the continuum method the recovery of the temperature is about 90%. Once again, it can be seen that the rotational temperature obtained by the DSMC method shows good agreement with Rothe's measured rotational temperature. In Fig. 15 is shown the effect of wall interaction models on the rotational temperature at $x/R_t = 18.7$, 3 mm inside from the nozzle exit, in the DSMC method. Four different gas/surface interaction models are considered: 1) diffuse reflection with full thermal accommodation, 2) diffuse reflection with no thermal accommodation (adiabatic wall), 3) diffuse reflection with 10% thermal accommodation, and 4) 70% diffuse—30% specular reflection. The DSMC result with diffuse reflection with 10% thermal accommodation at the wall shows the best agreement with the measured rotational temperature. Although not shown, the gas/surface interaction models considered here have a negligible effect on the density profile, except for the specular reflection that results in a faster expansion of the flow, i.e., higher axial velocity, lower density and temperature inside the nozzle.

Conclusions

A low-density nozzle flow is analyzed by two different approaches, the continuum method based on a finite volume approximation of the Navier-Stokes equations, which are based on continuum gas dynamics, and the DSMC method based on molecular gasdynamics. The results are compared with Rothe's experimental density and rotational temperature values that were measured at various locations inside the nozzle. Comparison of results from the two methods with the experimental data show that the continuum method can provide

relatively good results inside the nozzle as far as density is concerned. The results from the DSMC method show good agreement with the experimental data, both in the density and the rotational temperature. It is also shown that the simulation parameters, such as the gas/surface interaction model, the energy exchange model between rotational and translational modes, and the viscosity-temperature exponent, have substantial effects on the results of the DSMC method, and a proper choice of these parameters is very important for more accurate results. These parameters are largely dependent on the kind of propellant and surface materials, and more accumulation of experimental data bases are required on this subject.

Acknowledgments

Support by the NASA Lewis Research Center, Cleveland, Ohio, under Grant NCC 3-171 and Contract NAS 3-25266 is gratefully acknowledged.

References

[1]Bird, G. A., *Molecular Gas Dynamics*, Oxford Univ. Press, London, 1976.

[2]Bird, G. A., "The Nozzle Lip Problem," *Rarefied Gas Dynamics*, edited by M. Becker and M. Fiebig, DFVLR Press, Porz-Wahn, Germany, 1974, pp. A. 22 1–8.

[3]Bird, G. A., "Breakdown of Continuum Flow in Freejets and Rocket Plumes," *Rarefied Gas Dynamics*, edited by S. S. Fisher, AIAA, New York, 1981, pp. 681–694.

[4]Hueser, J. E., Melfi, L. T., Jr., Bird, G. A., and Brock, F. J., "Rocket Nozzle Lip Flow by Direct Simulation Monte-Carlo Method," *Journal of Spacecraft*, Vol. 23, No. 4, 1986, pp. 363–367.

[5]Campbell, D. H., "Nozzle-Lip Effects on Argon Expansions into the Plume Backflow," *Journal of Spacecraft*, Vol. 26, No. 4, 1989, pp. 285–292.

[6]Campbell, D. H., "Angular Variation of Flowfield Properties in Free Jet Expansions," *Rarefied Gas Dynamics*, edited by A. E. Beylich, VCH Press, Weinheim, Germany, 1991, pp. 1019–1024.

[7]Nelson, D. A., and Doo, Y. C., "Simulation of Multicomponent Nozzle Flows into a Vacuum," *Rarefied Gas Dynamics*, edited by E. P. Muntz, D. P. Weaver, and D. H. Campbell, Vol. 116, Progress in Astronautics and Aeronautics, AIAA, Washington, DC, 1989, pp. 340–351.

[8]Penko, P. F., Boyd, I. D., Meissner, D. L., and De Witt, K. J., "Pressure Measurements in a Low-Density Nozzle Plume for Code Verification," AIAA Paper 91-2110, June 1991.

[9]Boyd, I. D., Penko, P. F., Meissner, D. L., and De Witt, K. J., "Experimental and Numerical Investigations of Low-Density Nozzle and Plume Flows of Nitrogen," *AIAA Journal*, Vol. 30, No. 10, 1992, pp. 2453–2461.

[10]Zelesnik, D., Dunn, T., Micci, M. M., and Long, L. N., "Numerical and Experimental Investigation of Low Reynolds Number Nozzle Flows," AIAA Paper 91-3558, Sept. 1991.

[11]Yoon, S., and Shuen, J. S., "A LU-SSOR Scheme for the Euler and Navier-Stokes Equations," AIAA Paper 87-0600, Jan. 1987.

[12]Shuen, J. S., and Yoon, S., "Numerical Study of Chemically Reacting Flows Using a Lower-Upper Symmetric Successive Overrelaxation Scheme," *AIAA Journal*, Vol. 27, No. 12, 1989, pp. 1752–1760.

[13]Rothe, D. E., "Electron Beam Studies of Viscous Flow in Supersonic Nozzles," *AIAA Journal*, Vol. 9, No. 5, 1972, pp. 804–811.

[14]Kim, S. C., and VanOverbeke, T. J., "Performance and Flow Calculations of Gaseous H_2/O_2 Thrusters," *Journal of Spacecraft and Rockets*, Vol. 28, No. 4, 1991, pp. 433–438.

[15]Kim, S. C., "Numerical Study of High-Area-Ratio H_2/O_2 Rocket Nozzles," AIAA Paper 91-2434, June 1991.

[16]Stubbs, R. M., Kim, S. C., and Benson, T. J., "Computational Fluid Dynamics Studies of Nuclear Rocket Performance," AIAA Paper 91-3557, Sept. 1991.

[17]Kim, S. C., "Calculations of Low Reynolds Number Rocket Nozzles," AIAA Paper 93-0888, Jan. 1993.

[18]Bird, G. A., "Monte Carlo Simulation in an Engineering Context," *Rarefied Gas Dynamics*, edited by S. S. Fisher, Vol. 74, Pt. I, Progress in Astronautics and Aeronautics, AIAA, New York, 1981, pp. 239–255.

[19]Bird, G. A., "The Perception of Numerical Methods in Rarefied Gas Dynamics," *Rarefied Gas Dynamics*, edited by E. P. Muntz, D. P. Weaver, and D. H. Campbell, Vol. 118, Progress in Astronautics and Aeronautics, AIAA, Washington, DC, 1989, pp. 211–226.

[20]Chung, C. H., Kim, S. C., Stubbs, R. M., and De Witt, K. J., "DSMC and Continuum Analyses of Low-Density Nozzle Flow," AIAA Paper 93-0727, Jan. 1993.

[21]Chung, C. H., Kim, S. C., Stubbs, R. M., and De Witt, K. J., "Analysis of Plume Backflow Around a Nozzle Lip in a Nuclear Rocket," AIAA Paper 93-2497, June 1993.

[22]Chung, C. H., Kim, S. C., De Witt, K. J., and Nagamatsu, H. T., "Numerical Analysis of Hypersonic Low-Density Scramjet Inlet Flow," *Journal of Spacecraft and Rockets* (to be published).

[23]Borgnakke, C., and Larsen, P. S., "Statistical Collision Models for Monte Carlo Simulation of Polyatomic Gas Mixture," *Journal of Computational Physics*, Vol. 18, No. 4, 1975, pp. 405–420.

[24]Boyd, I. D., "Analysis of Rotational Nonequilibrium in Standing Shock Waves of Nitrogen," *AIAA Journal*, Vol. 28, No. 11, 1990, pp. 1997–1999.

[25]Parker, J. G., "Rotational and Vibrational Relaxation in Diatomic Gases," *Physics of Fluids*, Vol. 2, No. 4, 1959, pp. 449–462.

[26]Lordi, J. A., and Mates, R. E., "Rotational Relaxation in Non-Polar Diatomic Gases," *Physics of Fluids*, Vol. 13, No. 2, 1970, pp. 291–308.

[27]Kohler, M., "Reibung in mäßig verdünnten Gasen als Folge verzögerter Einstellung der Energie," *Zeitschrift Für Physik*, Vol. 125, 1949, pp. 715–732.

[28]Brau, C. A., and Jonkman, R. A., "Classical Theory of Rotational Relaxation in Diatomic Gases," *Journal of Chemical Physics*, Vol. 52, No. 2, 1970, pp. 477–484.

[29]Belikov, A. E., Sukhinin, G. I., and Sharafutdinov, R. G., "Nitrogen Rotational Relaxation Time Measured in Freejets," *Rarefied Gas Dynamics*, edited by E. P. Muntz, D. P. Weaver, and D. H. Campbell, Vol. 117, Progress in Astronautics and Aeronautics, AIAA, Washington, DC, 1989, pp. 40–51.

[30]Prangsma, G. J., Alberga, A. H., and Beenakker, J. J. M., "Ultrasonic Determination of the Volume Viscosity of N_2, CO, CH_4, and CD_4 Between 77 and 300K," *Physica*, Vol. 64, 1973, pp. 278–288.

[31]Annis, B. K., and Malinauskas, A. P., "Temperature Dependence of Rotational Collision Numbers from Thermal Transpiration," *Journal of Chemical Physics*, Vol. 54, No. 11, 1971, pp. 4763–4768.

[32]Healy, R. N., and Storvick, T. S., "Rotational Collision Number and EuckenFactors from Thermal Transpiration Measurements," *Journal of Chemical Physics*, Vol. 50, No. 3, 1969, pp. 1419–1427.

[33]Carnevale, E. H., Carey, C., and Larson, G., "Ultrasonic Determination of Rotational Collision Numbers and Vibrational Relaxation Times of Polyatomic Gases at High Temperatures," *Journal of Chemical Physics*, Vol. 47, No. 8, 1967, pp. 2829–2835.

[34]Winter, T. G., and Hill, G. L., "High-Temperature Measurements of Rotational Relaxation in Hydrogen, Deuterium, Nitrogen, and Oxygen," *Journal of the Acoustical Society of America*, Vol. 4, No. 4, 1967, pp. 848–858.

[35]Malinauskas, A. P., "Thermal Transpiration. Rotational Relaxation Numbers for Nitrogen and Carbon Dioxide," *Journal of Chemical Physics*, Vol. 44, No. 3, 1966, pp. 1196–1202.

[36]Mason, E. A., "Molecular Relaxation Times from Thermal Transpiration Measurements," *Journal of Chemical Physics*, Vol. 39, No. 3, 1963, pp. 522–526.

[37]Camac, M., Avco Everett Research Lab. Res. Rept. 172, Everett, MA, Dec. 1963.

[38]Pettersson, J. B. C., Nyman, G., and Holmlid, L., "A Classical Trajectory Study of Inelastic Scattering of NO from Graphite Surfaces: Rotational Energy Distributions," *Journal of Chemical Physics*, Vol. 89, No. 11, 1989, pp. 6963–6971.

[39]Hama, F. R., "Experimental Investigations of Wedge Base Pressure and Lip Shock," Jet Propulsion Lab., California Inst. of Technology, TN-32-1033, Pasadena, CA, June 1966.

[40]Olsson, G. R., and Messiter, A. F., "Acceleration of a Hypersonic Boundary Layer Approaching a Corner," Univ. of Michigan, Willow Run Labs. of the Inst. of Science and Technology, Rept. 8416-13-T, Ann Arbor, MI, May 1968.

[41]Rothe, D. E., "Experimental Study of Viscous Low-Density Nozzle Flows," Cornell Aeronautical Lab., Inc., AI-2590-A-2, Buffalo, NY, June 1970.